PAPER

Check for updates

Synthesis and antibacterial effects of cobalt–cellulose magnetic nanocomposites

N. S. Alahmadi,[a] J. W. Betts,[b] F. Cheng,[a] M. G. Francesconi, [ID] [a] S. M. Kelly, [ID] *[a] A. Kornherr,[c] T. J. Prior[a] and J. D. Wadhawan*[d]

Green synthesis is employed to prepare cobalt/cellulose nanocomposites with cubic (α-cobalt) cobalt as a main component with antibacterial and magnetic properties. An *in situ* reduction of aqueous solutions of cobalt ions on a model cellulose substrate surface using hydrogen gas affords spherical, cellulose-stabilised cobalt nanoclusters with magnetic properties and an average diameter of 7 nm that are distributed evenly over the surface of the cellulose fibres. These cobalt/cellulose nanocomposites exhibit good antibacterial action against opportunistic pathogens both Gram-positive (*S. aureus*) and Gram-negative (*E. coli*, *A. baumannii* and *P. aeruginosa*), with zones of inhibition up to 15 mm, thereby encouraging the deployment of these advanced materials for the treatment of wastewater or within medical dressings. This method of preparation is compared with the analogous *in situ* reduction of cobalt ions on a cellulose surface using sodium borohydride as reducing agent.

Introduction

Magnetic nanoparticles have attracted attention due to their potential applications in a wide range of technologies, for example environmental remediation, catalysis, magnetic fluids and magnetic resonance imaging.[1–3] There are three main types of magnetic nanoparticles: pure metals, metal oxides and alloys.[4–6] Various synthetic approaches have been developed to synthesise magnetic nanoparticles, such as co-precipitation, sol–gel, chemical reduction, gas reduction, thermal decomposition, micelle synthesis and ultrasonic spray pyrolysis.[7–9] Chemical reduction in aqueous solution is a convenient and cost effective approach to prepare magnetic nanoparticles,[5,10] usually using strong reducing reagents, such as sodium and potassium borohydrides.[11–14]

However, this approach poses several challenges: magnetic nanoparticles are thermodynamically unstable due to the high surface energy and so they manifest a pronounced tendency to aggregate in order to minimise the effective surface energy.[3,14] For the solution-phase synthesis of magnetic metallic nanoparticles of cobalt, there are two further aspects to consider: first unwanted cobalt by-products may be generated during the reaction;[1,10,15] second, in the absence of a surfactant coating,

aerial oxidation of naked magnetic nanoparticles may result in a loss of magnetism.[1,11,16] Therefore, a successful synthesis of air-stable magnetic nanoparticles would be highly desirable, especially in terms of the potential benefits in handling and processing for practical applications.[10] One of the approaches to stabilise and protect magnetic nanoparticles from aggregation and oxidation is to coat them with either a thin organic layer, consisting of polymers or surfactants, for example, or an inert, inorganic coating, such as silica.[8,16–19]

Recently, a diverse range of green chemistry approaches to the synthesis of many kinds of nanoparticles has been developed in order to minimise the generation or utilisation of hazardous and toxic reagents and side products.[20–26] Cellulose has been used as an organic surface coating and stabiliser in such approaches due, to its combination of advantageous properties: it is naturally abundant, biodegradable and readily available at low cost.[27,28] Cellulose fibres can be combined with a wide variety of nanoparticles to create new cellulose nanocomposites, which may possess an advantageous combination of properties, such as magnetic, photo-catalytic antibacterial and electrically conductive properties.[27,29] Modified cellulose nanocomposites have been used as an adsorbent to remove heavy metals from water.[27,30] Furthermore, nanomagnetic cellulose could be a leading means to produce cheap devices for data storage and security purposes.[19,29] Moreover, for synthetic transformation cellulose and its derivatives often combine the roles of reducing agent, with stabiliser and solubiliser.[31,32]

There is a paucity of work published pertaining to the antibacterial activity of cobalt nanoparticles: almost all research has investigated complexes of cobalt and other metals/organic materials, such as zinc oxide and cobalt-doped zinc oxide

[a]*School of Mathematics & Physical Sciences, University of Hull, Cottingham Road, Kingston Upon Hull, HU6 7RX, UK. E-mail: s.m.kelly@hull.ac.uk*

[b]*School of Veterinary Medicine, University of Surrey, Daphne Jackson Road, Guildford, GU2 7AL, UK*

[c]*Mondi Uncoated Fine Paper, Haidmuehlstrasse 2-4, A-3363 Ulmerfeld-Hausmening, Austria*

[d]*School of Engineering & Computer Sciences, University of Hull, Cottingham Road, Kingston Upon Hull, HU6 7RX, UK. E-mail: j.wadhawan@hull.ac.uk*

nanoparticles.[33] However, very little data on the concentrations required for antibacterial action have been reported, and little difference in antibacterial activity has been observed between zinc oxide and cobalt-doped zinc oxide nanoparticles. It has been found that pure, irregular-shaped cobalt–ferrite nanoparticles show antibacterial action against *Staphylococcus aureus* and *Escherichia coli*.[34] However, zinc or cobalt-substituted cobalt–ferrite nanoparticles produced significantly greater antibacterial activity than the cobalt–ferrite nanoparticles alone. Cobalt–ferrite nanoparticles produce minimal antibacterial activity against several species of bacteria including *E. coli*, *S. aureus* and *Pseudomonas aeruginosa*.[35] This poor antibacterial action could be due to the ferrite complexes inhibiting the release of cobalt ions and thereby reducing the natural antibacterial action.

Metal nanoparticles have great importance in health and medicine, with metal and metal oxides being more stable at high temperatures and pressures than traditional organic antimicrobials.[36] The use of nanoparticles could have a significant impact on minimizing the transfer of bacteria, such as *S. aureus*, a constituent part of the natural skin flora and *E. coli*, part of the natural gut flora of the human body, between patients in a hospital environment. *S. aureus* and *E. coli* are opportunistic pathogens responsible for serious infections, which can often be treated with broad-spectrum antibiotics. However, due to the growing concern of antimicrobial resistance, alternative antimicrobials are needed. Hospital infections can occur in immune-suppressed or immune-compromised individuals, such as the elderly, patients with cancer or HIV/AIDS and post-operative patients.[37,38] Infection leads to extensive hospital stays, resulting in increased healthcare costs and increased patient morbidity/mortality.

Accordingly, the prevention of infections caused by bacteria could reduce patient mortality and associated treatment costs. Antibacterial coatings of cobalt nanoparticles with a large active surface area on cellulose bandages, uniforms, bed linen, surfaces and medical equipment could make a significant contribution to reducing bacterial transfer and also preventing injury, or elective surgery-related wound infections.

In this work, we present a new green approach to the synthesis and stabilization of pure cobalt nanoparticles with antibacterial, as well as magnetic, properties using cellulose as a stabilizer and sodium borohydride or hydrogen gas as the reducing agent. The antibacterial effect of these nanoparticles on bacterial pathogens is investigated.

Experimental

Chemicals

Cellulose paper samples of 1 mm thickness, were generously provided as a gift from Mondi Uncoated Fine Paper, Austria. Cobalt(II) nitrate hexahydrate (Co(NO$_3$)$_2$·6H$_2$O, purity $\geq$ 98.0%), sodium borohydride (NaBH$_4$, purity $\geq$ 98.0%) were purchased from Sigma Aldrich, UK. Ethanol was purchased from Fisher Scientific, UK. All reagents were used without further purification. Hydrogen and nitrogen gas were obtained from BOC (UK). Cellulose paper was dried overnight at room temperature and under vacuum conditions. All other reagents were dried to

remove any adventitious or bound water prior to their use. All aqueous reaction solutions were prepared using doubly deionised and filtered water with a resistivity greater than 18 MΩ cm at a temperature of 20 $\pm$ 3 °C. Liquids (water, aqueous solutions and ethanol) were oxygen-purged with impurity-free nitrogen immediately prior to reaction.

Bacterial type strains used in this investigation: *Staphylococcus aureus* ATCC 25923, *Escherichia coli* ATCC 12241, *Acinetobacter baumannii* ATCC 19606 and *Pseudomonas aeruginosa* ATCC 27853 were purchased from the Public Health England bacterial collections laboratory (Colindale, UK). All dehydrated culture media was purchased from Oxoid (Basingstoke, UK) and autoclaved prior to experimentation.

Procedures

The synthesis of cobalt nanoparticles was conducted under anaerobic conditions within a bespoke containment facility exploiting a nitrogen blanket. Specific procedures are outlined below.

Synthesis of cobalt cellulose nanocomposites using NaBH$_4$ as a reducing agent

An aqueous solution (20 ml) of cobalt(II) nitrate (0.1 M) was placed in a sealed three-necked round bottom flask, which contained a sample of cellulose paper (100 mg), at room temperature and incubated for three minutes, after which the solution was discarded, and the paper sample rinsed with degassed ethanol for *ca.* 30 s. Subsequently, the cellulose paper was incubated for ten minutes with 20 ml of an aqueous 0.2 M sodium borohydride solution. The cellulose paper was then rinsed with water (one minute) and dried at room temperature *in vacuo*. The nucleated cobalt metal nanoparticles obtained through the reduction of cobalt ions by sodium borohydride were subsequently enabled to grow through heating the modified cellulose paper within a tube furnace with inert gases, either N$_2$ or H$_2$ at 165 °C for 8 h. These protocols were repeated through altering the cobalt(II) concentration in aqueous solution from 0.1 M, and through changing the reduction time from ten minutes, as indicated in the Results & discussion section.

Synthesis of cobalt cellulose nanocomposites using H$_2$ as a reducing agent

An aqueous solution (20 ml) of cobalt(II) nitrate (0.1 M) was placed in a sealed three-necked round bottom flask, which contained a sample of cellulose paper (100 mg), at room temperature and incubated for three minutes, after which the solution was discarded, and the paper sample rinsed with degassed ethanol for *ca.* 30 s. The cobalt(II) ions were reduced in a stream of hydrogen gas at 200 °C for 20 h. These protocols were repeated through altering the cobalt(II) concentration in aqueous solution from 0.1 M to 1.0 M.

Characterisation of the cobalt cellulose nanocomposites

The cobalt content within the nanoparticle-modified cellulose nanocomposite was obtained using inductively coupled plasma

mass spectrometry (ICP-MS, Perkin Elmer DRC ICP MS ultra-trace metal analyser).

The structure of the cobalt nanoparticles within the nano-composite samples was characterised using powder X-ray diffraction (PXRD), using a diffractometer (Siemens D 5000) fitted with an Ni-filter, emitting at Cu K_α, ($\lambda = 0.154$ nm), using an airtight sample holder. The samples were loaded into the sample holder under an inert atmosphere.

The morphology of the cobalt–cellulose nanocomposite samples were obtained from images captured during transmission electron microscopy (TEM) with an Ultra Scan 4000 digital camera (Gatan UK, Abingdon) attached to a Jeol 2010 transmission electron microscope (Jeol UK Ltd. Welwyn Garden City) running at 120 kV. The diameters of the nanoparticles features were estimated using ImageJ software. EDX spectra were obtained using an INCA X-sight system running through INCA Analyser software (Oxford Instruments, High Wycombe, UK).

Antibacterial assays

Individual Iso-Sensitest agar plates were inoculated with isolates of *S. aureus* (ATCC 25923), *E. coli* (ATCC 12241), *A. baumannii* (ATCC 19606) and *P. aeruginosa* (ATCC 27853) using a standardized method.[39] Cellulose/nanoparticle nano-composites were added to individual inoculated agar plates (10^5 colony forming units [CFU] ml^{-1}), which were then incubated at 37 °C for 24 h. This process was repeated for cellulose-stabilised cobalt nanoclusters as powders, which were coated onto blank, sterile paper discs (0.5 mg per disc surface) before being added to inoculated agar plates. Blank sterile papers were also used as controls.

The antibacterial activity of these samples was evaluated using a method based on that by Pollini *et al.*[40] Zones of inhibition surrounding the coated samples were measured and the antibacterial action was rated "good" (zone of inhibition > 1 mm), "fairly good" (zone of inhibition ≤ 1 mm), "sufficient" (growth up to, but not on, the paper sample), "limited" (limited growth on the paper sample) or "poor" (paper sample is over-grown with bacteria ≥ 50%).

Results and discussion

Synthesis of cobalt cellulose nanocomposites

In undertaking the synthetic procedure, the initially cream-coloured cellulose paper, first developed a pink colouration, as the result of adsorption of the cobalt ions onto the surface of the cellulose fibres. Then, the cellulose paper rapidly turned black on the addition of the reducing agent (hydrogen gas or a sodium borohydride solution), which is indicative of the reduction of cobalt ions. The rate of the reduction reaction increased, evidenced through the time taken for the cellulose to blacken, at higher temperature of reaction. The paper remained a black colour after drying in vacuum. Samples subsequently heated under a stream of either hydrogen or nitrogen exhibit either a deeper black or brown colour, respectively (inhomogeneous colour) and also exhibit some magnetic properties, see

Fig. 1. The black colour and magnetic properties are a strong indication for the presence of metallic cobalt nanoparticles on the cellulose samples. Some of the samples developed a green, rather than a black or brown colour and lost their magnetic properties over time on exposure to air, which is strongly indicative of oxidation of the surface of the metallic cobalt nanoparticles to cobalt oxide.

Table 1 records the amount of cobalt in the cobalt/cellulose nanocomposite samples as determined using ICP analysis. The first set of data, samples 1–5, represents the *in situ* synthesis of cobalt nanoclusters, using sodium borohydride as the reducing agent. The quantity of cobalt and boron in the samples increased with increasing concentrations of the reaction precursors. Increasing the reduction time led to the same trend. Surprisingly, sample 3 contains lower concentrations of cobalt and boron than that in other samples (samples 2 and 4). This probably erroneous phenomenon may be due to a significant loss of these elements during washing with either ethanol or water. The cellulose-stabilised cobalt nanoclusters appear, generally, to be fixed to the cellulose fibre surface of the other samples and are not removed by repeated washing with water.

The concentrations of cobalt in the second group of samples 6–9, synthesised by reduction of cobalt ions with hydrogen gas, also increase with the concentration of cobalt ions in the reaction solution as expected. The contamination of the samples 6–9 with boron is negligible. These results indicate that pure, cellulose-stabilised, metallic cobalt nanoclusters are formed on the fibre surface of the cobalt/cellulose nanocomposites 6–9 prepared using hydrogen gas as reducing agent.

The PXRD patterns of the cobalt/cellulose nanocomposites as received and after heating under nitrogen or hydrogen are shown in Fig. 2. Surprisingly, no peaks attributable to hexagonal (β-cobalt) cobalt or cubic (α-cobalt) can be observed amongst the peaks for cellulose, although these samples show
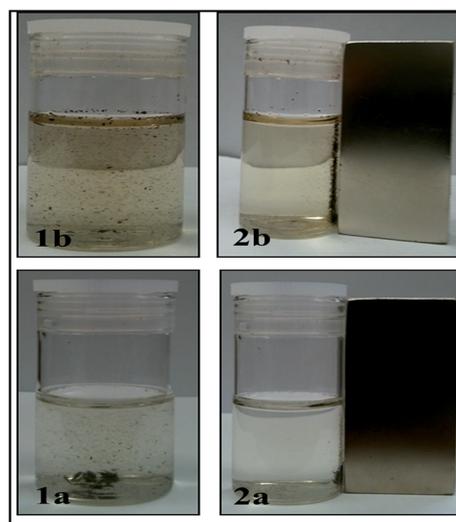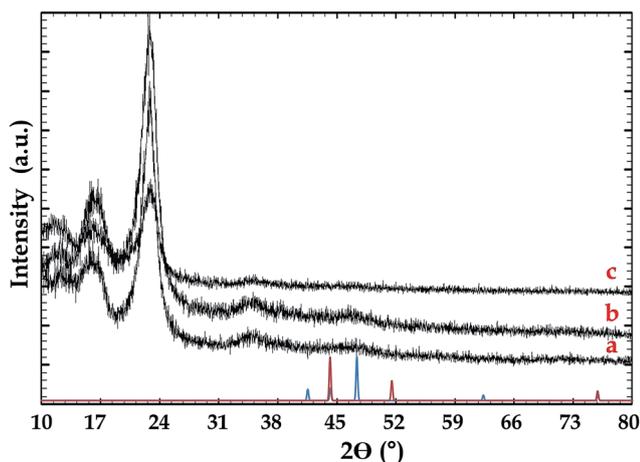

Fig. 1 Photographs of the effects of attraction between the cobalt/cellulose nanocomposites and a magnet. 1(a) and 2(a) sample 5 and 1(b) and 2(b) sample 9, synthesised from reduction of cobalt ions using either sodium borohydride or hydrogen gas, respectively.

Table 1 The reaction conditions for the preparation of the cobalt cellulose/nanocomposites 1–5 or 6–9 produced by using either reduction with sodium borohydride or hydrogen gas, respectively, as the reducing agent and the concentration of metallic cobalt and boron in the samples 1–9

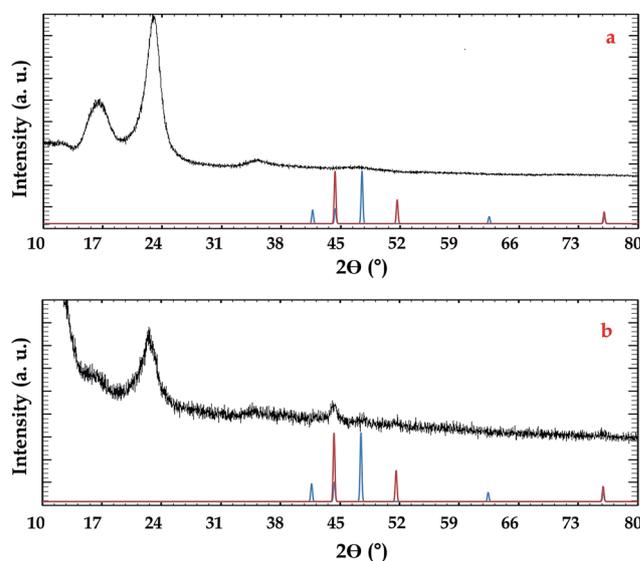| Samples	Concentration, M		Volume, ml		Conditions		% w/w	
	Co^{2+}	BH_4^-	Co^{2+}	BH_4^-	Temp. °C	Time, min	Co	B
1	0.1	0.2	15	15	N_2 RT	10	0.51	2.04
2	0.1	0.2	20	20	N_2 RT	10	1.10	0.12
3	0.1	0.2	20	20	N_2 RT	20	0.57	0.075
4	0.1	0.2	20	20	N_2 RT	30	2.25	0.21
5	1	2	20	20	N_2 RT	10	5.88	3.98
6	0.1	0	20	0	H_2 200	1200	1.99	0.016
7	0.4	0	20	0	H_2 200	1200	4.25	0.006
8	0.7	0	20	0	H_2 200	1200	4.54	0.000
9	1	0	20	0	H_2 200	1200	5.01	−0.002

magnetic properties, see Fig. 1. ICP analysis indicates the presence of significant amounts of boron in the samples 1–5 and residual amounts of boron in the samples 6–9 (Table 1). Cobalt boride (Co_2B) should be formed as the primary product in these reactions.[10,41] It has also been suggested that the cobalt boride formed initially could react with more cobalt to produce cobalt boride (Co_3B).[42,43] Co_2B could also be converted to other compounds, e.g., $Co(BO_2)_2$ and $Co_3(BO_3)_2$.[41,44] However, no peaks for these compounds can be observed in the XRD patterns. One possible explanation for this finding is that the cobalt metal and the cobalt boron complexes in the cobalt cellulose nanocomposites may be amorphous. Another possible reason is that any small peaks, potentially attributable to cobalt metal and cobalt boron complexes, are masked by the large cellulose peaks due to the low concentration of cobalt and boron as shown in Table 1. Heating of the samples under N_2 or H_2 flow at 165 °C for 8 h does not lead to the observation of any cobalt peaks in the PXRD patterns. The PXRD patterns are similar for other samples prepared at different concentration of starting materials or at different reaction times (not shown).

Fig. 3 displays the PXRD patterns of cobalt/cellulose nanocomposites prepared by hydrogen gas reduction of different concentration cobalt ions at 200 °C for 20 h. The PXRD pattern of the sample prepared from 0.1 M of $Co(NO_3)_2$ shows no peaks other than cellulose peaks as the content of cobalt is too low to be determined in the nanocomposite (Fig. 3a). Increasing the concentration of $Co(NO_3)_2$ to 1.0 M, facilitates the observation of weak peaks ascribed to the formation of cobalt metal, with cubic (α-cobalt) cobalt as a main component.[47,48] No other peaks from cobalt–boron complexes can be observed, consistent with the ICP results shown in Table 1.

Fig. 4 shows TEM images of the cobalt/cellulose nanocomposites, the corresponding size distribution of the nanoclusters as well as the results of elemental analysis using EDX. As can be seen in Fig. 4a, spherical cobalt nanoclusters with a diameter of 2.5 ± 0.7 nm can be observed for the

Fig. 2 PXRD pattern for cobalt/cellulose nanocomposites 1–5. Black patterns are experimental data: (a) sample as received, (b) sample after heating under N_2, (c) sample after heating under H_2. Lines are reference data: blue lines are a hexagonal structure of cobalt; red lines are a cubic structure of cobalt.[45,46]

Fig. 3 PXRD of cobalt/cellulose nanocomposites 6–9 prepared at different concentrations of cobalt ions, reduced by hydrogen gas. Black patterns: 3(a) 0.1 M of $Co(NO_3)_2$; 3(b) 1 M of $Co(NO_3)_2$. Reference data: the blue lines are characteristic of a hexagonal crystal structure of cobalt[45] and red lines are characteristic of a cubic crystal structure of cobalt.[46]
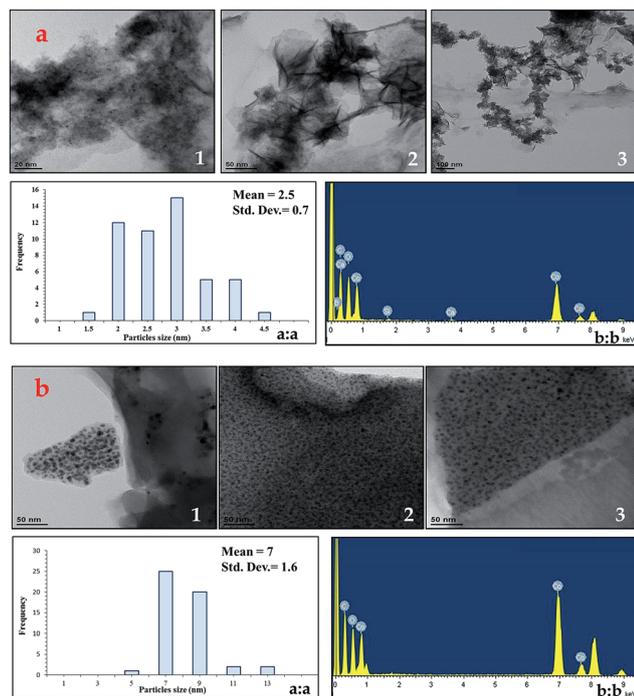
Fig. 4 TEM images of cobalt/cellulose nanocomposites prepared using different reducing agents, their corresponding size distribution and elemental analysis by EDX. 4(a) Sample 5 and 4(b) sample 9 synthesised from reduction of cobalt ions using sodium borohydride and hydrogen gas, respectively.

nanocomposites 1–5, synthesised by sodium borohydride reduction. These small metallic nanoclusters aggregate on the cellulose fibre surface to form much larger, amorphous aggregates without any characteristic shape or form. Elemental analysis using EDX reveals the presence of metallic cobalt in the samples 1–5. Although the results of ICP analysis indicate the presence of boron in these samples, a peak attributable to boron is not evident in the EDX spectra, which is probably attributable to an overlap between the boron and the carbon peaks. In the nanocomposites 6–9, prepared using hydrogen gas reduction, see Fig. 4b, larger spherical nanoclusters, with a diameter of 7 ± 1.6 nm, than those determined for the nanocomposites 1–5 synthesised by sodium borohydride

reduction, see Fig. 4a, are observed. The greater diameter may be due to the fact that hydrogen reductions were carried out at 200 °C, rather than at room temperature, as was the case for the sodium borohydride reductions. The cellulose-stabilised cobalt nanoclusters appear to be homogenously distributed on the surface of the cellulose fibres. The larger surface area and the presence of cellulose may help prevent aggregation and agglomeration of the cobalt nanoclusters in the samples 6–9. The high reaction temperature may have also induced further growth of the cobalt nanoclusters. The elemental analysis using EDX suggests that boron is not present in the samples 6–9, in agreement with ICP results recorded in Table 1.

Antibacterial assays

The results of the antibacterial assays are collated in Table 2. The cobalt/cellulose nanocomposites produce good antibacterial action against all bacterial isolates tested, with the size of the zone of inhibition greater than 1 mm. Samples 7–9, prepared using hydrogen gas reduction, produce the greatest antibacterial activity against all of the bacterial species tested with the zone of inhibition reaching a diameter of up to 15 mm against *S. aureus* (Fig. 5) and 14 mm against *E. coli* (Fig. 6a). Cellulose alone produces no antibacterial activity and samples are overgrown with bacteria (Fig. 6b). *S. aureus* and *E. coli* are the most susceptible, with all samples producing good activity, with the exception of sample 6/2, which still generates sufficient activity against the bacteria. The cobalt/cellulose nanocomposites are least effective against *A. baumannii*, although antibacterial activity is observed for each sample tested. Lower susceptibility is probably due to metal ion resistance mechanisms, such as active efflux.

There are several potential mechanisms for the antibacterial action observed. Highly reactive oxygen species (ROS), such as hydrogen peroxide, can be formed in the presence of metallic nanoclusters and air, resulting in substantial damage to bacterial DNA, cell membranes (lipid peroxidation) and protein dysfunction.[49,50] Equally, cobalt ions released from metallic cobalt nanoclusters can interact with thiol groups on essential bacterial enzymes, resulting in their inactivation and leading to cell death. Another potential mode of action is through impaired membrane function, which is thought to be due to electrostatic interaction of the metal nanoparticles and the

Table 2 Antibacterial effects of the cobalt/cellulose nanocomposites, 2 and 5, synthesised by sodium borohydride reduction, and the corresponding samples 6–9, synthesised by hydrogen gas reduction, along with a control sample[a]

	Bacterial pathogens			
Samples	*S. aureus* 25923	*E. coli* 12241	*A. baumannii* 19606	*P. aeruginosa* 27853
2	1 mm good	0 mm sufficient	0 mm sufficient	0 mm sufficient
5	5 mm good	5 mm good	0 mm sufficient	1 mm good
6	0 mm sufficient	1 mm good	0 mm sufficient	0 mm sufficient
7	12 mm good	10 mm good	2 mm good	7 mm good
8	12 mm good	14 mm (good)	1 mm good	5 mm good
9	15 mm good	10 mm good	5 mm good	2 mm good

[a] Zones of inhibition are presented as the diameter of the area of no bacterial growth, minus the diameter of the sample itself.
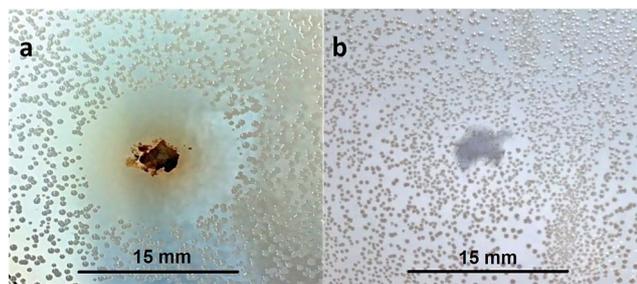
Fig. 5 (a) Antibacterial action of the cobalt/cellulose nanocomposite sample 9 producing a zone of inhibition of 15 mm against *S. aureus* ATCC 25923 and (b) of cellulose alone showing bacterial overgrowth.
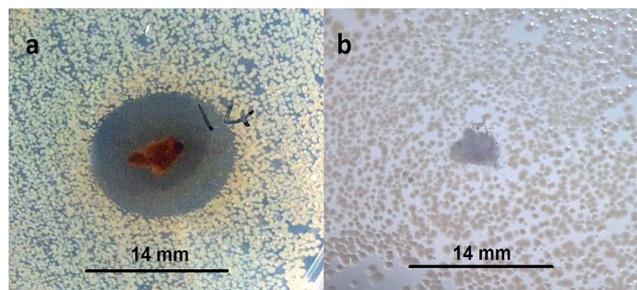

Fig. 6 (a) Antibacterial action of the cobalt/cellulose composite sample 8 producing a zone of inhibition of 14 mm against *E. coli* ATCC 12241 and (b) of cellulose alone showing bacterial overgrowth.

surface of the bacteria. This results in aggregation of nanoclusters on the cell surface and changes in cell morphology, leading to growth inhibition. Each of these potential mechanisms has greater potency for metallic nanoclusters than for metallic macroparticle/solid metal surfaces, due to the greater active surface area of the metallic nanoclusters, associated with a highly reactive surface. This leads to greater interactions with cells and the release of higher concentrations of metal ions.[51] Cobalt resistance has mainly been described in *Alcaligenes* spp. and *Ralstonia* spp. although it has also been observed for *E. coli via* CzcABC efflux pumps.[52] However, cobalt nanocomposite resistance in this study was not observed, as evidenced by the fact that all the cobalt/cellulose nanocomposite samples tested produce sufficient/good antibacterial action against each of the bacterial species tested.

Conclusions

A green synthetic approach to prepare cobalt/cellulose nanocomposites with antibacterial and magnetic properties has been developed by *in situ* reduction of cobalt ions on the substrate surface using hydrogen gas. Spherical, cellulose-stabilised cobalt metallic nanoclusters with an average diameter of 7 nm are formed with cubic cobalt (α-cobalt) as a main component. The cellulose-stabilised, metallic cobalt nanoclusters are homogenously distributed on the surface of the cellulose fibres. The cobalt/cellulose nanocomposites are contaminated with almost insignificant traces of boron. In

contrast, *in situ* reduction of cobalt ions on cellulose surface with sodium borohydride gives amorphous cobalt/cellulose composites with a significant contamination with boron. All of the cobalt/cellulose nanocomposites show good antibacterial action against the bacterial isolates tested. A detailed investigation of the magnetic properties of these nanocomposites and the dependence of antibacterial action on the nanocomposite concentration will be the focus of future work.

Acknowledgements

Notes and references

1 A.-H. Lu, E. L. Salabas and F. Schüth, *Angew. Chem., Int. Ed.*, 2007, **46**, 1222–1244.
2 W. Baaziz, S. Begin-Colin, B. P. Pichon, I. Florea, O. Ersen, S. Zafeiratos, R. Barbosa, D. Begin and C. Pham-Huu, *Chem. Mater.*, 2012, **24**, 1549–1551.
3 A. Gual, C. Godard, S. Castillon, D. Curulla-Ferre and C. Claver, *Catal. Today*, 2012, **183**, 154–171.
4 Y. Sui, L. Yue, R. Skomski, X. Z. Li, J. Zhou and D. J. Sellmyer, *J. Appl. Phys.*, 2003, **93**, 7571–7573.
5 T. Hyeon, *Chem. Commun.*, 2003, 927–934.
6 M. Giersig and M. Hilgendorff, *J. Phys. D: Appl. Phys.*, 1999, **32**, L111–L113.
7 S. Gurmen, S. Stopic and B. Friedrich, *Mater. Res. Bull.*, 2006, **41**, 1882–1890.
8 X. G. Lu, G. Y. Liang, Z. B. Sun and W. Zhang, *Mater. Sci. Eng., B*, 2005, **117**, 147–152.
9 Y. P. Bao, W. An, C. H. Turner and K. M. Krishnan, *Langmuir*, 2010, **26**, 478–483.
10 C. S. S. R. Kumar, *Magnetic Nanomaterials*, Wiley-VCH, Weinheim, 2009.
11 I. Narita, T. Oku, H. Tokoro and K. Suganuma, *Solid State Commun.*, 2006, **137**, 44–48.
12 T. Oku, I. Narita and H. Tokoro, *J. Phys. Chem. Solids*, 2006, **67**, 1152–1156.
13 I. Markova-Deneva, *J. Chem. Technol. Metall.*, 2010, **45**, 351–378.
14 C. Burda, X. B. Chen, R. Narayanan and M. A. El-Sayed, *Chem. Rev.*, 2005, **105**, 1025–1102.
15 A. H. Lu, E. L. Salabas and F. Schuth, *Angew. Chem., Int. Ed.*, 2007, **46**, 1222–1244.
16 H. Bönnemann, W. Brijoux, R. Brinkmann, N. Matoussevitch, N. Waldöfner, N. Palina and H. Modrow, *Inorg. Chim. Acta*, 2003, **350**, 617–624.
17 S. P. Gubin, Y. A. Koksharov, G. B. Khomutov and G. Y. Yurkov, *Russ. Chem. Rev.*, 2005, **74**, 489–520.
18 K. Landfester and L. P. Ramirez, *J. Phys.: Condens. Matter*, 2003, **15**, S1345–S1361.

19 J. A. Carrazana-Garcia, M. A. Lopez-Quintela and J. R. Rey, *IEEE Trans. Magn.*, 1995, **31**, 3126–3130.

20 O. V. Kharissova, H. V. R. Dias, B. I. Kharisov, B. O. Perez and V. M. J. Perez, *Trends Biotechnol.*, 2013, **31**, 240–248.

21 D. Nath and P. Banerjee, *Environ. Toxicol. Pharmacol.*, 2013, **36**, 997–1014.

22 R. S. Varma, *Curr. Opin. Chem. Eng.*, 2012, **1**, 123–128.

23 F. Cheng, J. W. Betts, S. M. Kelly and A. L. Hector, *Mater. Sci. Eng., C*, 2015, **46**, 530–537.

24 F. Cheng, J. W. Betts, S. M. Kelly, J. Schaller and T. Heinze, *Green Chem.*, 2013, **15**, 989–998.

25 F. Cheng, J. W. Betts, S. M. Kelly, D. W. Wareham, A. Kornherr, F. Dumestre, J. Schaller and T. Heinze, *J. Mater. Chem. B*, 2014, **2**, 3057–3064.

26 P. Raveendran, J. Fu and S. L. Wallen, *J. Am. Chem. Soc.*, 2003, **125**, 13940–13941.

27 A. M. Donia, A. A. Atia and F. I. Abouzayed, *Chem. Eng. J.*, 2012, **191**, 22–30.

28 J. Kim, S. Yun and Z. Ounaies, *Macromolecules*, 2006, **39**, 4202–4206.

29 J. Shen, Z. Q. Song, X. R. Qian and Y. H. Ni, *Ind. Eng. Chem. Res.*, 2011, **50**, 661–666.

30 O. Karnitz, L. V. A. Gurgel, R. P. de Freitas and L. F. Gil, *Carbohydr. Polym.*, 2009, **77**, 643–650.

31 Z. G. Li, A. Friedrich and A. Taubert, *J. Mater. Chem.*, 2008, **18**, 1008–1014.

32 J. Cai, S. Kimura, M. Wada and S. Kuga, *Biomacromolecules*, 2009, **10**, 87–94.

33 M. G. Nair, M. Nirmala, K. Rekha and A. Anukaliani, *Mater. Lett.*, 2011, **65**, 1797–1800.

34 N. Sanpo, C. C. Berndt, C. Wen and J. Wang, *Acta Biomater.*, 2013, **9**, 5830–5837.

35 M. Kooti, S. Saiahi and H. Motamedi, *J. Magn. Magn. Mater.*, 2013, **333**, 138–143.

36 Y. Liu, L. He, A. Mustapha, H. Li, Z. Q. Hu and M. Lin, *J. Appl. Microbiol.*, 2009, **107**, 1193–1201.

37 H. Lee, Y.-S. Lee, R. Jeong, Y.-J. Kim and S. Ahn, *Infection*, 2014, **42**, 669–674.

38 A. Senthilkumar, S. Kumar and J. N. Sheagren, *Clin. Infect. Dis.*, 2001, **33**, 1412–1416.

39 F. Moosdeen, J. D. Williams and A. Secker, *J. Antimicrob. Chemother.*, 1988, **21**, 439–443.

40 M. Pollini, M. Russo, A. Licciulli, A. Sannino and A. Maffezzoli, *J. Mater. Sci.: Mater. Med.*, 2009, **20**, 2361–2366.

41 G. N. Glavee, K. J. Klabunde, C. M. Sorensen and G. C. Hadjapanayis, *Langmuir*, 1992, **8**, 771–773.

42 U. B. Demirci and P. Miele, *Phys. Chem. Chem. Phys.*, 2010, **12**, 14651–14665.

43 G. N. Glavee, K. J. Klabunde, C. M. Sorensen and G. C. Hadjipanayis, *Langmuir*, 1993, **9**, 162–169.

44 A. K. Srivastava, S. Madhavi, T. J. White and R. V. Ramanujan, *J. Mater. Chem.*, 2005, **15**, 4424–4428.

45 L. J. E. Hofer and W. C. Peebles, *J. Am. Chem. Soc.*, 1947, **69**, 893–899.

46 A. Taylor and R. W. Floyd, *Acta Crystallogr.*, 1950, **3**, 285–289.

47 V. F. Puntes, K. M. Krishnan and P. Alivisatos, *Appl. Phys. Lett.*, 2001, **78**, 2187–2189.

48 S. Sun, C. B. Murray and H. Doyle, *Mater. Res. Soc. Symp. Proc.*, 1999, **577**, 385–398.

49 T. D. Rae, P. J. Schmidt, R. A. Pufahl, V. C. Culotta and T. V. O'Halloran, *Science*, 1999, **284**, 805–808.

50 K. Kon and M. Rai, *J. Comp. Clin. Path. Res.*, 2013, **2/1**, 160–174.

51 K. Senior, S. Muller, V. J. Schacht and M. Bunge, *Recent Pat. Food, Nutr. Agric.*, 2012, **4**, 200–209.

52 D. H. Nies, *J. Bacteriol.*, 1995, **177**, 2707–2712.